Designer spin systems via inverse statistical mechanics

Robert A. DiStasio, Jr.,[1] Étienne Marcotte,[2] Roberto Car,[1,2,3,4] Frank H. Stillinger,[1] and Salvatore Torquato[1,2,3,4]

[1]*Department of Chemistry, Princeton University, Princeton, New Jersey 08544, USA*

[2]*Department of Physics, Princeton University, Princeton, New Jersey 08544, USA*

[3]*Princeton Institute for the Science and Technology of Materials, Princeton University, Princeton, New Jersey 08544, USA*

[4]*Program in Applied and Computational Mathematics, Princeton University, Princeton, New Jersey 08544, USA*

In this work, we extend recent inverse statistical-mechanical methods developed for many-particle systems to the case of spin systems. For simplicity, we focus in this initial study on the two-state Ising model with radial spin-spin interactions of finite range (i.e., extending beyond nearest-neighbor sites) on the square lattice under periodic boundary conditions. Our interest herein is to find the optimal set of shortest-range pair interactions within this family of Hamiltonians, whose corresponding ground state is a targeted spin configuration such that the difference in energies between the energetically closest competitor and the target is maximized. For an exhaustive list of competitors, this optimization problem is solved exactly using linear programming. The possible outcomes for a given target configuration can be organized into the following three solution classes: unique (nondegenerate) ground state (class I), degenerate ground states (class II), and solutions not contained in the previous two classes (class III). We have chosen to study a general family of striped-phase spin configurations comprised of alternating parallel bands of up and down spins of varying thicknesses and a general family of rectangular block checkerboard spin configurations with variable block size, which is a generalization of the classic antiferromagnetic Ising model. Our findings demonstrate that the structurally anisotropic striped phases, in which the thicknesses of up- and down-spin bands are equal, are unique ground states for isotropic short-ranged interactions. By contrast, virtually all of the block checkerboard targets are either degenerate or fall within class III solutions. The degenerate class II spin configurations are identified up to a certain block size. We also consider other target spin configurations with different degrees of global symmetries and order. Our investigation reveals that the solution class to which a target belongs depends sensitively on the nature of the target radial spin-spin correlation function. In the future, it will be interesting to explore whether such inverse statistical-mechanical techniques could be employed to design materials with desired spin properties.

I. INTRODUCTION

In statistical mechanics, the Ising model[1] is used to describe the fundamental physics underlying the phenomenon of ferromagnetism in materials. In its simplest form, the Ising model consists of a two-state spin system, in which the individual spins (representing magnetic dipole moments) are arranged on a lattice and either aligned or antialigned ($\sigma = \pm 1$) with respect to an arbitrary external reference direction. In the absence of an external magnetic field, the individual spins interact via a nearest-neighbor potential described by the following Hamiltonian:

$$\mathcal{H}(J) = -J \sum_{\langle ij \rangle} \sigma_i \sigma_j, \qquad (1)$$

in which $\langle ij \rangle$ denotes a restriction of the summation to include only the unique pairs of spins i and j that are nearest neighbors, and J is the spin-spin coupling constant or interaction strength parameter.

More generalized Ising spin models are made possible by specifying the manifold of allowed spin states, the spatial arrangement of the spin array, and the set of interactions present in the system. For instance, the set of allowed spin states can be extended from the discrete two-state (up-/down-) spin system comprising the simplest Ising model to a continuous vector representation, in which the individual spins can point in essentially any direction, as found in the q-state Potts, Heisenberg, and classical XY models.[2–6] Second, the variables

specifying the geometrical and topological arrangement of the spin system include the choice of the global system dimensionality [one dimensional (1D), two dimensional (2D), three dimensional (3D), . . .], the underlying lattice (linear, triangular, cubic, etc.), and the boundary conditions employed (periodic, antiperiodic, etc.); a judicious specification of these variables facilitates the study of several additional fundamental physical phenomena, such as order-disorder phase transitions, symmetry breaking, and spontaneous magnetization. To complete the description of a generalized Ising spin model, the set of interactions present in the system must be specified in terms of the functional form of the potential (radial, two-body, three-body, . . .), the spatial extent of the interactions (nearest neighbor, next-nearest neighbor,[7,8] etc.), the range and magnitude of the spin coupling constants, and the presence of any external magnetic fields.

Allowing for specification of the aforementioned variables defines the following class of Hamiltonians, with the flexibility to describe any generalized Ising spin system:

$$
\begin{aligned}
\mathcal{H}(\{J\},\{h\}) = &-\sum_{i<j} J_2(\mathbf{R}_i,\mathbf{R}_j) f_2(\mathbf{R}_i,\mathbf{R}_j,\sigma_i,\sigma_j) \\
&- \sum_{i<j<k} J_3(\mathbf{R}_i,\mathbf{R}_j,\mathbf{R}_k) \\
&\times f_3(\mathbf{R}_i,\mathbf{R}_j,\mathbf{R}_k,\sigma_i,\sigma_j,\sigma_k) \\
&- \cdots - \sum_i h(\mathbf{R}_i)\sigma_i, \qquad (2)
\end{aligned}
$$

in which $f_2, f_3, \ldots$ represent the functional form of the two-body, three-body, $\ldots$ spin interaction potentials in terms of the coordinates $\{\mathbf{R}\}$ and allowed states $\{\sigma\}$ of the spins comprising the system, $J_2, J_3, \ldots$ denote the corresponding spin interaction strength parameters, and h are the spin-field coupling constants governing the interactions of individual spin sites with an external magnetic field.

Over the past century, a tremendous amount of work has been dedicated to solving the standard, or "forward," problem of statistical mechanics for the Ising model and generalizations thereof.[1,6,9–14] Given a Hamiltonian such as those found in Eqs. (1) and (2), one computes the structural and bulk properties (e.g., expectation values, correlation functions, thermodynamic functions, etc.) corresponding to the spin system of interest.

By contrast, little to no attention has been focused to date on "inverse" problems within the context of the Ising spin models, in which the problem proceeds in reverse, i.e., given a targeted spin configuration to be a desired state of matter (e.g., a ground or excited state, or a system endowed with novel bulk properties), one seeks to procure the Hamiltonian (or class of Hamiltonians) describing the optimal underlying set of interactions that will lead to the prescribed *target* system. In fact, several promising techniques for solving the inverse problem have recently emerged in the literature and were initially applied to classically interacting many-particle systems to produce unusual ground states[15–18] as well as unique bulk properties at positive temperatures.[19,20] To the best of our knowledge, this paper describes the first application of inverse methods developed by us to spin systems.

To address the inverse spin problem, the variables described above must first be specified to fully delineate the generalized Ising spin system of interest (and the corresponding class of Hamiltonians). In this work, we consider a generalization of the simple two-state Ising model presented above that extends the interaction potential beyond nearest-neighbor spin sites, allowing for radial pair interactions between spins of varying separations. As an initial application, we examined spin systems arranged on a square lattice, subject to standard periodic boundary conditions along both the x and y axes (i.e., square $\mapsto$ 2D torus), in the absence of an external magnetic field. Further generalizations of the spin interaction potential and the underlying lattice will be reserved for future work.

The class of Hamiltonians describing the generalized Ising spin model considered herein is therefore parametrized by a set of distance-dependent spin-spin coupling strengths, i.e.,

$$\mathcal{H}(\{J\}) = -\sum_{i<j} J(R_{ij})\sigma_i \sigma_j, \qquad (3)$$

in which $R_{ij} = |\mathbf{R}_i - \mathbf{R}_j|$ is the radial distance between spins i and j.[21]

For a given periodic system with a unit cell containing N spins, it is convenient to define the $\mathbf{S}_2$ vector, a quantity that is closely related to the spin-spin correlation function,[22] with components (labeled by R) given by

$$S_2(R) \equiv \frac{1}{N} \sum_{i<j} \sigma_i \sigma_j \delta_{R,R_{ij}}, \qquad (4)$$

in which $\delta_{R,R_{ij}}$ is the Kronecker delta. The magnitude of $S_2(R)$ assumes a maximum absolute value $S_2^{\max}(R)$, when all of the spins separated by a distance R are either aligned or antialigned, reflecting the coordination degeneracy associated with the given radial interspin separation [see Eq. (8) below].

This formalism allows for direct computation of the energy per spin ϵ for a given spin configuration via

$$\epsilon \equiv \frac{E}{N} = -\sum_R J(R)S_2(R) = -\mathbf{J} \cdot \mathbf{S}_2, \qquad (5)$$

i.e., the scalar product of $\mathbf{S}_2$ with $\mathbf{J}$, the vector containing the distance-dependent spin-spin coupling strengths. Hence, for a given vector $\mathbf{J}$, a trivial lower (upper) bound on the energy per spin is attained by

$$\epsilon_{\text{bound}} = -\sum_R J(R)S_2^{\max}(R), \qquad (6)$$

when both $J(R)$ and $S_2^{\max}(R)$ have the same (opposite) sign for all radial interspin separations included in the above summation. Since the $J(R)$ are the parameters specifying the class of Hamiltonians in Eq. (3), the solution of the inverse spin problem is attained by finding the optimal set of $J(R)$ corresponding to a target spin configuration, i.e., the spin-spin interaction potential that yields the target as a possible unique (nondegenerate) ground state.

In the search for the optimal spin-spin interaction potential corresponding to a desired target spin configuration, several possible outcomes emerge and can be organized into the following three solution classes:

Class I: Solutions in which a spin-spin interaction potential was found that generates the target spin configuration as a *unique* (nondegenerate) ground state up to translations, rotations, reflections, and spin inversion operations.

Class II: Solutions in which a spin-spin interaction potential was found that generates the target spin configuration as a *nonunique* ground state, with degenerate spin configurations having the same $\mathbf{S}_2$ as the target ($\mathbf{S}_2$-type degeneracies).

Remark: $\mathbf{S}_2$-type degeneracies remain isoenergetic for *any* choice of the spin-spin interaction potential [cf. Eq. (5)].

Class III: Solutions that are not contained in either class I or II as defined above.

Remark: It should be emphasized that a target spin configuration corresponding to a class III solution does not necessarily mean that this spin configuration can not be the ground state corresponding to any radial pairwise interaction potential. For instance, this solution class designation could correspond to finding an interaction potential which generates the target spin configuration as a *nonunique* ground state that is energetically degenerate with spin configurations that do not have the same $\mathbf{S}_2$ correlation function (non-$\mathbf{S}_2$-type degeneracies).[23]

In this initial exploration of the inverse problem in discrete spin systems, we chose to systematically examine two fundamental families of spin systems as target spin configurations. The first set of target spin systems considered herein is the sequence of striped-phase spin configurations, which are comprised of alternating stripes (or bands) of aligned spins of varying thickness; throughout this work, the striped-phase
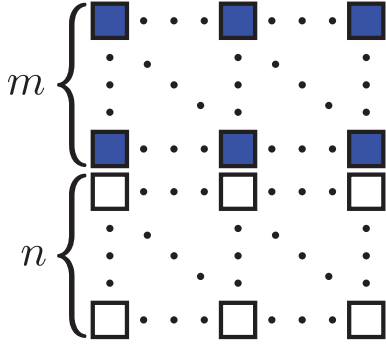
FIG. 1. (Color online) Graphical depiction of the SP[m,n] striped-phase spin configuration. The blue and white boxes represent the two-state spin projection values (up/down) discretized on the square lattice.

FIG. 2. (Color online) Graphical depiction of the CB[m,n] block checkerboard spin configuration. The blue and white boxes represent the two-state spin projection values (up/down) discretized on the square lattice.

spin configurations will be denoted as SP[m,n], in which m and n refer to the thickness (in the number of spins) of the alternating stripes as illustrated in Fig. 1.

Striped phases are common patterns that form spontaneously in nature and are found in a variety of materials, including (ultra)thin magnetic films,[24–27] physisorbed,[28] Langmuir,[29] and lipid[30] monolayers, liquid crystals,[31] and polymer films,[32] to name a few. Tailoring the electronic and magnetic properties of materials that contain striped phases has many direct technological applications, in particular to the fields of nanolithography and nanoelectricity, i.e., the development of novel materials for information storage, quantum dots, high-temperature superconductivity,[33–35] as well as functional oxide heterostructures for use in solid oxide fuel cells.[36] Therefore, an *a priori* understanding of the underlying interactions necessary to generate and stabilize striped phases in materials, which can be attained utilizing the inverse statistical-mechanical techniques described herein, would prove invaluable in the design of striped molecular architectures. To date, all of the interaction potentials that have been shown to stabilize striped-phase spin configurations in the literature require long-range (dipolarlike) interactions;[37–40] in this work, we have uncovered the fact that radial pairwise spin-spin interaction potentials with a finite range will also yield striped-phase spin configurations as unique ground states, a finding that provides further insight into the stability and formation of striped-phase materials. Such spin systems can be viewed as the lattice analogs of the "striped-phase" ground states achieved in many-particle systems with short-ranged, radial pair potentials.[15,41]

The second set of target spin systems considered herein is the sequence of rectangular block checkerboard spin configurations, which are generalizations of the classic antiferromagnetic Ising spin configuration (i.e., the *simple* checkerboard); throughout this work, the block checkerboard spin configurations will be denoted as CB[m,n], in which m and n refer to the height and width (in the number of spins) of the blocks as illustrated in Fig. 2. The block checkerboard spin configurations, or more appropriately, the lattice-gas analogs thereof, provide us with model systems to study materials with varying pore sizes, which are prevalent in biochemistry and
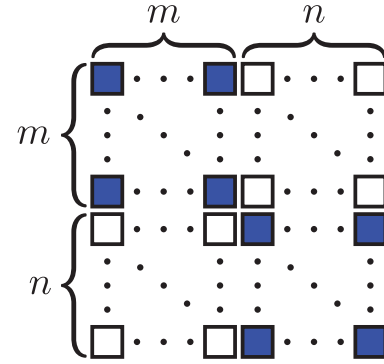
biophysics (ion channels, transport proteins, cell membranes) as well as the energy sciences (metal organic frameworks).

The remainder of the paper is organized as follows. In Sec. II, we describe the inverse statistical-mechanical methods utilized in this work to obtain numerical solutions for the inverse spin problem. In Sec. III, we present the results of our systematic study of the striped-phase and block checkerboard spin configurations, as well as some other illustrative examples. Section IV contains an in-depth discussion of the mapping between spin configurational space and the $\mathbf{S}_2$ spin-spin correlation function for the nearest-neighbor and next-nearest-neighbor spin-spin interaction potentials. The paper is then completed in Sec. V, which provides some brief conclusions as well as the future outlook of the inverse spin problem.

II. METHODS

In this section, we describe the competitor-based zero-temperature optimization scheme[15,16,42] that has been utilized in this work to obtain numerical solutions to the inverse problem for the aforementioned spin systems. Given a target spin configuration $\mathcal{T}$, the goal of this optimization scheme is to furnish the *shortest-range* spin-spin interaction potential that favors the target spin configuration by energetically disfavoring all possible competitors, thereby yielding the target as a possible unique (nondegenerate) ground state (class I solution). This spin-spin interaction potential corresponds to the set of $J(R)$ that maximizes $\Delta\epsilon^k = \epsilon^{C_k} - \epsilon^{\mathcal{T}}$, the difference in energy per spin between the energetically closest competitor C_k and the target, over the entire set of available competitors.

Obtaining this potential is achieved via global optimization of z, the corresponding objective function:

$$z \equiv \max_{\mathbf{J}} \left[\min_{C_k} [\Delta\epsilon^k] \right]$$

$$= \max_{\mathbf{J}} \left[\min_{C_k} \left[-\sum_R J(R) \left[S_2^{C_k}(R) - S_2^{\mathcal{T}}(R) \right] \right] \right], \quad (7)$$

subject to the constraints that $\Delta\epsilon^k \geqslant 0 \; \forall \; k$ and the set of $J(R)$ are bounded within the interval $[-1, +1]$ for every allowed radial distance R. On an infinite square lattice, these radial

interspin separations are provided by the corresponding theta series[43]

$$\theta(q) = 1 + 4q + 4q^2 + 4q^4 + 8q^5 + 4q^8 + \cdots \qquad (8)$$

from which the exponents and coefficients yield the allowed values of R^2 ($R = 0, 1, \sqrt{2}, 2, \sqrt{5}, 2\sqrt{2}, \ldots$) and associated coordination degeneracies (1,4,4,4,8,4, . . .), respectively.

The construction of spin-spin interaction potentials according to the competitor-based zero-temperature optimization scheme described above relies on a feedback loop between (i) the global optimization of the objective function z in Eq. (7) and (ii) the generation of an adaptively modified set of competitor spin configurations $\{C_k\}$. Since z is a linear objective function [i.e., the energy per spin differences are linear in the $J(R)$ variables] subject to linear constraints, the highly efficient linear programming (LP) optimization technique[44] was employed to maximize z exactly (i.e., to machine precision) and generate the spin-spin interaction potentials. To construct the constantly evolving set of possible competitors, the simulated annealing (SA) optimization scheme[45] in conjunction with classical single spin-flip (Metropolis) Monte Carlo (MC) simulations were utilized to locate energetically relevant competitor spin configurations.

To initiate the algorithm utilized to carry out this competitor-based optimization scheme, a target spin configuration, a set of initial competitors (at least one), and a maximum radial distance $R_{\max}$ must be specified. In a sequential loop over the allowed radial interspin separations $R' \leqslant R_{\max}$ given by Eq. (8), the algorithm proceeds as follows:

Step 1. For the given radial distance R', the LP optimization scheme generates a potential $\{J(R)\}$ with a maximum radial extent of R' such that $\epsilon^{\mathscr{T}} < \epsilon^{C_k} \ \forall \ k$, *if such a potential exists.*

Step 2. Using SA-MC simulations, this potential is then employed to find a new competitor (or set of competitors) C_{k+1} such that $\epsilon^{C_{k+1}} \leqslant \epsilon^{\mathscr{T}}$, *if such a competitor exists.*

Steps 1 and 2 are then iterated until either of the following conditionals are met:

(i) For a given set of competitors, the LP procedure is unable to generate a potential that energetically favors the target [i.e., consider a longer-ranged interaction potential; move to next allowed radial interspin separation]. GO TO Step 1

(ii) For a given potential, the SA-MC procedure is unable to locate a new competitor that is lower (or degenerate) in energy compared to the target [i.e., a tentative optimal shortest-range interaction potential was located; begin potential verification protocol described below]. EXIT

Unless otherwise specified, the optimized spin-spin interaction potentials obtained by the competitor-based zero-temperature optimization scheme described above were generated and carefully verified using SA-MC simulations on all lattices with side lengths $1 \leqslant p \leqslant q \leqslant 40$ (i.e., including the series of 2D rectangular primary cells). For each interaction potential, the SA-MC verification runs were repeated until the corresponding *target* spin configuration (and any of its possible $\mathbf{S}_2$-type degeneracies) were successfully obtained 100 times (without finding any alternative spin configurations that were lower than or equal to in energy per spin relative to the target spin configuration).

III. RESULTS

A. SP[n,n] striped-phase spin configurations

The sequence of striped-phase (SP[n,n]) spin configurations, which are comprised of alternating stripes (or bands) of aligned spins of *equal* thickness (see Fig. 1), was the first set of spin configurations considered in this work as targets for the inverse spin problem. In particular, we systematically studied the effect of uniformly increasing the thickness of these alternating stripes in the series of SP[n,n] spin configurations for $n = 1, 2, \ldots, 10$. Using the competitor-based zero-temperature optimization scheme described in Sec. II, it was determined that *all* of the SP[n,n] spin configurations considered herein are unique ground-state spin configurations (class I solutions). Furthermore, the fact that this sequence of striped-phase spin configurations was deemed unique ground states (class I solutions) ensures that no other spin configurations characterized by the same $\mathbf{S}_2$ exist (i.e., there are no $\mathbf{S}_2$-type degeneracies for the SP[n,n] spin configurations). The set of optimized radial spin-spin interaction potentials $\{J(R)\}$ as well as the corresponding $\{S_2(R)\}$ values for a subset of the SP[n,n] spin configurations are provided in Table I.

The *shortest* radial interaction potentials necessary to generate the SP[n,n] spin configurations are of length n (i.e., the width of a stripe) in the interspin separation, with the exception of SP[1,1], the simplest striped-phase spin configuration, which requires an interaction potential extending to next-nearest neighbors ($R = \sqrt{2}$). Since $\mathbf{S}_2 = (0, -2)$ for the SP[1,1] spin configuration (see Table I), there is no nearest-neighbor component of the interaction potential that can energetically favor this spin configuration over the spectrum of competitors; as such, the interaction potential in this case extends further to include antiferromagnetic next-nearest-neighbor interactions at full interaction strength, i.e., with $J(\sqrt{2}) = -1$. In doing so, this interaction potential maximizes the energetic stabilization provided by next-nearest-neighbor interactions in the SP[1,1] spin configuration, which has an extremal $S_2(\sqrt{2}) = -2 = -S_2^{\max}(\sqrt{2})$ value; this alone is enough to maximize the energetic gap between the target SP[1,1] spin configuration and *all* other competitors, thereby producing the SP[1,1] spin configuration as a unique ground state (class I solution). However, the possession of an extremal value of $S_2(R)$ for a given interspin separation is not a prerequisite for a spin configuration to be a unique ground state. With the exception of the SP[1,1] spin configuration just discussed, none of the SP[n,n] spin configurations for $n = 2, 3, \ldots, 10$ have $\mathbf{S}_2$ vectors with extremal values for $R \leqslant n$ (see Table I), yet all of these spin configurations are unique ground states.

Another interesting point to note here is that the optimized radial interaction potentials generated in this work for the SP[n,n] spin configurations offer an alternative to the competing short-range ferromagnetic and long-range antiferromagnetic (dipolarlike) interactions that are also known to generate striped-phase spin configurations as unique ground states.[37–40] Evidently, radial two-body interaction potentials extending only to length n will also suffice in generating the SP[n,n] striped-phase spin configurations as unique ground states. As such, these finite-range interactions (i.e., having compact support) are discrete by construction and fundamentally differ

TABLE I. Optimized radial spin-spin interaction potentials $J(R)$, corresponding $S_2(R)$ values, and energies per spin (ϵ) for the series of SP[n,n] striped-phase spin configurations with $n = 1,2,\ldots,7$. For reference, $S_2^{\max}(R)$, the maximum allowed values of $S_2(R)$ for the given interspin separations, are provided in the column furthest to the right.

R^2	SP[1,1] $J(R)$	SP[1,1] $S_2(R)$	SP[2,2] $J(R)$	SP[2,2] $S_2(R)$	SP[3,3] $J(R)$	SP[3,3] $S_2(R)$	SP[4,4] $J(R)$	SP[4,4] $S_2(R)$	SP[5,5] $J(R)$	SP[5,5] $S_2(R)$	SP[6,6] $J(R)$	SP[6,6] $S_2(R)$	SP[7,7] $J(R)$	SP[7,7] $S_2(R)$	$S_2^{\max}(R)$
1	0.000	0	1.000	1	1.000	4/3	1.000	3/2	1.000	8/5	1.000	5/3	1.000	12/7	2
2	-1.000	-2	-0.500	0	1.000	2/3	1.000	1	1.000	6/5	1.000	4/3	1.000	10/7	2
4			-0.250	0	1.000	2/3	1.000	1	1.000	6/5	1.000	4/3	1.000	10/7	2
5					-0.333	0	0.000	1	1.000	8/5	1.000	2	1.000	16/7	4
8					-0.667	$-2/3$	1.000	0	1.000	2/5	1.000	2/3	1.000	6/7	2
9					-0.333	0	1.000	1/2	1.000	4/5	1.000	1	1.000	8/7	2
10							0.000	0	0.750	4/5	1.000	4/3	1.000	12/7	4
13							-1.000	-1	-1.000	0	-1.000	2/3	0.000	8/7	4
16							-1.000	0	1.000	2/5	1.000	2/3	1.000	6/7	2
17									0.500	0	0.994	2/3	1.000	8/7	4
18									1.000	$-2/5$	1.000	0	1.000	2/7	2
20									-1.000	$-4/5$	-1.000	0	0.833	4/7	4
25									-1.000	$-8/5$	1.000	$-1/3$	1.000	4/7	6
26											-1.000	0	1.000	4/7	4
29											-1.000	$-2/3$	-1.000	0	4
32											0.299	$-2/3$	1.000	$-2/7$	2
34											-1.000	$-4/3$	-1.000	$-4/7$	4
36											-0.833	0	1.000	2/7	2
37													-1.000	0	4
40													-1.000	$-4/7$	4
41													-1.000	$-8/7$	4
45													-1.000	$-8/7$	4
49													-1.000	0	2
ϵ	-2.000		-1.000		-3.111		-5.000		-9.800		-11.463		-17.905		

from the aforementioned infinite-range interactions (i.e., having infinite support) originating from continuous dipolarlike (inverse power) functions. In the future, it would also be interesting to investigate the solution classes and optimized interaction potentials corresponding to 3D slabs (i.e., the analogs of the 2D striped phases considered herein), which have already been studied in the context of such competing short- and long-range interactions.[40]

B. CB[n,n] block checkerboard spin configurations

The sequence of block checkerboard (CB[n,n]) spin configurations, which are comprised of alternating blocks of aligned spins of *equal* height and width (see Fig. 2), were the second set of spin configurations considered in this work as targets for the inverse spin problem. Again, we systematically studied the effect of uniformly increasing the height and width of these alternating blocks in the series of CB[n,n] spin configurations for $n = 1,2,\ldots,10$. Unlike the SP[n,n] spin configurations, which were found to be unique ground-state spin configurations (class I solutions), we found that *all* of the CB[n,n] spin configurations considered herein, with the exception of the classic CB[1,1] simple checkerboard, are nonunique ground-state spin configurations (class II solutions). This is most likely due to the fact that the CB[n,n] spin configurations have more radial isotropy than the SP[n,n] spin configurations; hence, the chances of finding other spin configurations with the same S_2 correlation function as the CB[n,n] spin configurations are greatly increased. The set of optimized radial spin-spin

interaction potentials $\{J(R)\}$ determined using the competitor-based zero-temperature optimization scheme described above, as well as the corresponding $\{S_2(R)\}$ values, are provided in Table II for a subset of the CB[n,n] spin configurations. Similar to the SP[n,n] spin configurations, the *shortest* radial interaction potentials necessary to generate the CB[n,n] spin configurations are also of length n (i.e., the height and width of a block) in the interspin separation.

As class II solutions, the CB[n,n] spin configurations for $n \geqslant 2$ are nonunique ground states with degenerate spin configurations having the same $\mathbf{S}_2$ for *all* interspin separations (i.e., $\mathbf{S}_2$-type degeneracies). As such, these $\mathbf{S}_2$-type degeneracies remain isoenergetic for *any* choice of the spin-spin interaction potential [cf. Eq. (5)]. Graphical depictions of these $\mathbf{S}_2$-type degeneracies are provided in Figs. 3 and 4 for the CB[2,2] and CB[4,4] spin configurations, respectively. The $\mathbf{S}_2$-type degeneracies for the CB[n,n] spin configurations with $n \geqslant 2$ are diagonal spin configurations which result from elementary transformations on the base CB[n,n] block checkerboard spin configurations (see Appendix B for further details about the $\mathbf{S}_2$-type degeneracies of the CB[n,n] block checkerboard spin configurations). Furthermore, the number of $\mathbf{S}_2$-type degeneracies for the CB[n,n] spin configurations $g(n)$ was found as

$$g(n) = 1 + \frac{\lfloor \frac{n}{2} \rfloor \left(\lfloor \frac{n}{2} \rfloor + 1 \right)}{2}, \qquad (9)$$

TABLE II. Optimized radial spin-spin interaction potentials $J(R)$, corresponding $S_2(R)$ values, and energies per spin (ϵ) for the series of CB[n,n] block checkerboard spin configurations with $n = 1, 2, \ldots, 6$. For reference, $S_2^{\max}(R)$, the maximum allowed values of $S_2(R)$ for the given interspin separations, are provided in the column furthest to the right.

	CB[1,1]		CB[2,2]		CB[3,3]		CB[4,4]		CB[5,5]		CB[6,6]		
R^2	$J(R)$	$S_2(R)$	$J(R)$	$S_2(R)$	$J(R)$	$S_2(R)$	$J(R)$	$S_2(R)$	$J(R)$	$S_2(R)$	$J(R)$	$S_2(R)$	$S_2^{\max}(R)$
1	-1.000	-2	0.000	0	1.000	2/3	1.000	1	1.000	6/5	1.000	4/3	2
2			0.000	0	0.222	2/9	-0.750	1/2	-1.000	18/25	1.000	8/9	2
4			-1.000	-2	-1.000	$-2/3$	1.000	0	1.000	2/5	1.000	2/3	2
5					0.889	$-4/9$	-0.375	0	0.000	12/25	-0.585	8/9	4
8					0.222	2/9	1.000	0	-0.059	2/25	0.712	2/9	2
9					-1.000	-2	-1.000	-1	-1.000	$-2/5$	-0.040	0	2
10							0.125	-1	-0.618	$-12/25$	-1.000	0	4
13							-0.125	0	1.000	$-4/25$	0.462	0	4
16							-1.000	-2	-1.000	$-6/5$	-1.000	$-2/3$	2
17									-0.088	$-36/25$	0.294	$-8/9$	4
18									-0.118	2/25	-0.612	0	2
20									-0.324	$-12/25$	0.446	$-4/9$	4
25									-1.000	$-38/25$	-1.000	$-4/3$	6
26											0.712	$-16/9$	4
29											0.272	$-8/9$	4
32											0.681	2/9	2
34											-0.322	0	4
36											-1.000	-2	2
ϵ	-2.000		-2.000		-3.037		-3.500		-4.405		-4.711		

in which $\lfloor \ldots \rfloor$ denotes the integer floor function [see Fig. 5 for a plot of $g(n)$ versus n for the series of CB[n,n] spin configurations]. From Eq. (9), it is clear that asymptotically the number of $\mathbf{S}_2$-type degeneracies for the CB[n,n] spin configurations increases quadratically with n.

Each $\mathbf{S}_2$-type degeneracy corresponding to a given CB[n,n] spin configuration has a different entropy or corresponding number of microstates (i.e., the number of spin configurations that are strictly degenerate after application of the complete set of unique symmetry transformations). For example, the number of microstates for each of the four $\mathbf{S}_2$-type degeneracies of the CB[4,4] spin configuration depicted in Fig. 4 were computed as (*clockwise from upper left-hand corner*): 32, 128, 128, and 32. We note in passing that the odds of successfully obtaining these degenerate structures using SA-MC simulations may not precisely match the above
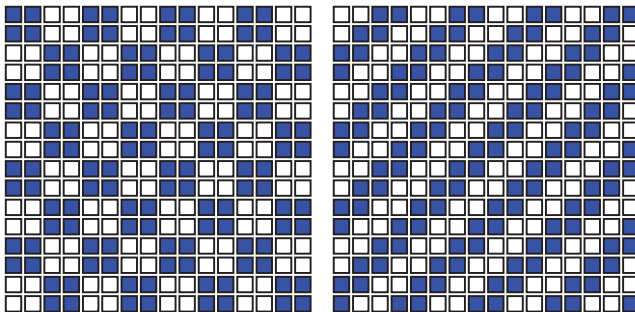
number of microstates, as the outcomes of these simulations strongly depend on the choice of the annealing schedule (i.e., finite-temperature effects) and the system size (on which one
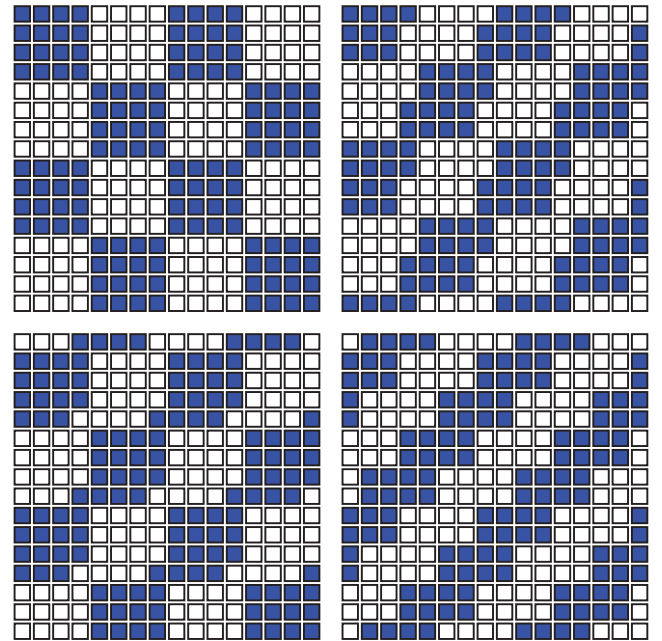

FIG. 4. (Color online) Class II $\mathbf{S}_2$-type degenerate structures for the CB[4,4] block checkerboard spin configuration. The CB[4,4] block checkerboard spin configuration has four $\mathbf{S}_2$-type degeneracies: CB$_{00}$[4,4] (upper left panel), CB$_{21}$[4,4] (upper right panel), CB$_{11}$[4,4] (lower left panel), and CB$_{22}$[4,4] (lower right panel).

FIG. 3. (Color online) Class II $\mathbf{S}_2$-type degenerate structures for the CB[2,2] block checkerboard spin configuration. The CB[2,2] block checkerboard spin configuration has two $\mathbf{S}_2$-type degeneracies: CB$_{00}$[2,2] (left panel) and CB$_{11}$[2,2] (right panel).
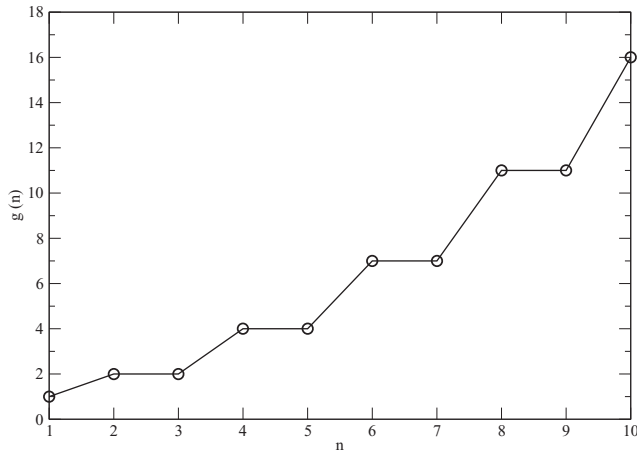
FIG. 5. Plot of the number of S_2-type degeneracies $g(n)$ as a function of system size n for the series of class II CB[n,n] block checkerboard spin configurations [cf. Eq. (9) and Appendix B].

is performing the SA-MC simulations). For more details, see the phase behavior (thermodynamics) comments in Sec. V.

C. SP[m,n] striped-phase and CB[m,n] block checkerboard spin configurations

Solution of the full inverse statistical-mechanical problem for more complex *target* spin configurations requires a significant amount of computational resources due to the large number and wide variety of possible competitor spin configurations that must be considered during optimization of the corresponding spin-spin interaction potential. However, the solution class corresponding to a particular *target* spin configuration can be determined by restricting the simulated annealing step, the rate-limiting process in the competitor-based zero-temperature optimization scheme described above, to a small subset of lattice sizes (determined by the periodicity of the *target* spin configuration) in the search for possible competitor spin configurations (see Appendix A for a detailed explanation). Figure 6 showcases the results of such an investigation for the sequence of striped-phase (SP[m,n]) and block checkerboard (CB[m,n]) spin configurations in which $1 \leqslant m \leqslant 5$ and $m \leqslant n \leqslant 15$.

In our study of the SP[n,n] and CB[n,n] spin configurations presented in Secs. III A and III B, respectively, we found that CB[1,1] and all of the SP[n,n] spin configurations were class I solutions, while the CB[n,n] spin configurations (for $n \geqslant 2$) were class II solutions. Extending this study to include the SP[m,n] and CB[m,n] spin configurations, we found that the SP[m,n] and CB[m,n] spin configurations *both* admit class III solutions that follow the same pattern: a spin configuration is a class III solution if and only if $n/m \in \mathbb{Z} \geqslant 3$. For all other n/m ratios, the SP[m,n] and CB[m,n] spin configurations have the same class structure as their $m = n$ analogs. Interestingly, this classification pattern depends solely on the geometrical ratio between n and m, has no dependence on the (periodic) length scale of the spin configurations, and is shared between these two seemingly distinct sets of spin configurations.

These findings suggest the possibility of a continuum limit, in which certain geometrical patterns, such as those exhibited in the SP and CB spin configurations, can be stabilized using long-range interactions. Since both the SP[m,n] and CB[m,n] spin configurations consist of alternating regions of uniformly oriented spins, this classification pattern may be indicative of the limitations of a radial pairwise interaction potential in stabilizing certain spin configurations with two inherently distinct length scales. However, the intriguing observation that radial pairwise interactions can not stabilize certain length scales (i.e., the aforementioned integer ratios) might simply be a consequence of the relatively small number of parameters (one for each allowed radial interspin separation) that define the interaction potentials considered in this work; the degree of flexibility afforded by these parameters simply does not allow the optimization procedure to take advantage of the slight differences between which radial interspin separations should have ferromagnetic interactions and which ones should have antiferromagnetic interactions.

D. Other target spin configurations

In addition to the series of striped-phase and block checkerboard spin configurations discussed above, we also considered several other target spin configurations during this initial study of the inverse spin problem. A select subset of these target spin configurations will be presented in this section, which includes (a) the set of diamond wallpaper
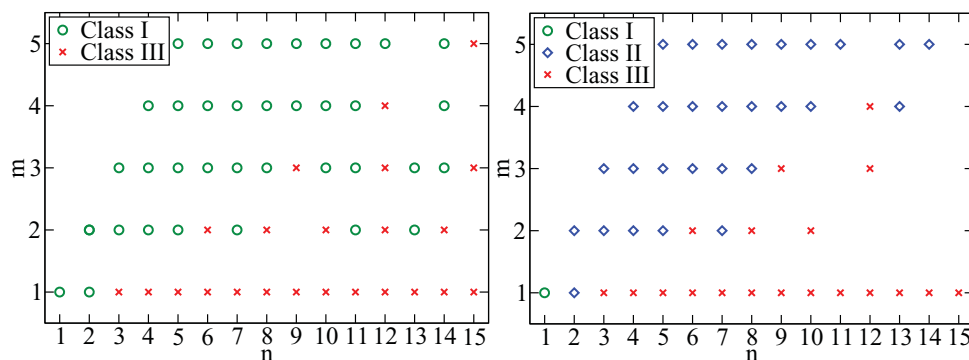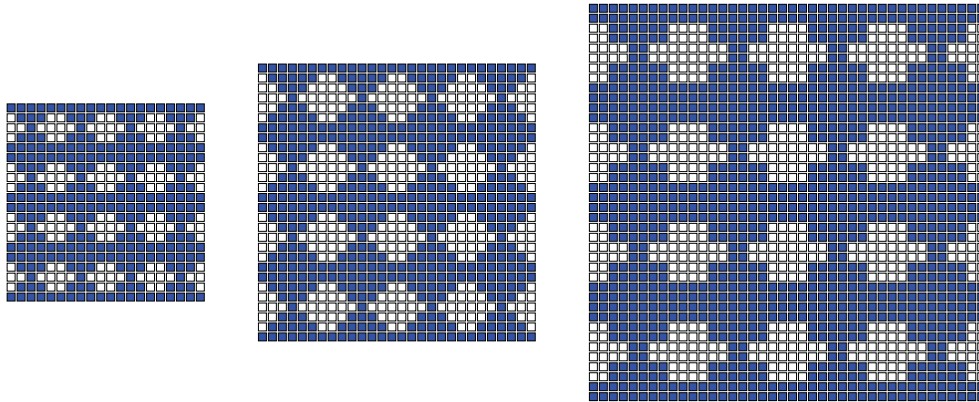

FIG. 6. (Color online) Solution classes for the (a) SP[m,n] striped-phase and (b) CB[m,n] block checkerboard spin configurations, for which $1 \leqslant m \leqslant 5$ and $m \leqslant n \leqslant 15$. The results for spin configurations with $n < m$ were omitted from the figure due to the fact that the SP[m,n] (CB[m,n]) spin configurations are identical to the SP[n,m] (CB[n,m]) spin configurations up to translational symmetry operations.

FIG. 7. (Color online) Graphical depiction of the set of diamond wallpaper spin configurations (D[I] − D[III]) considered in this work. From left to right, the resolution of the central diamond pattern is increased via discretization into blocks containing 8 (D[I]), 18 (D[II]), and 24 (D[III]) spins.

spin configurations, (b) a simple discretized asymmetric facial pattern, and (c) the simplest spin configuration corresponding to a class III solution.

The set of diamond wallpaper spin configurations D[I] − D[III] represent systematic changes in the resolution of a given discretized spin pattern and is depicted in Fig. 7. Considering D[I] as the "base" spin configuration, in which the diamond pattern is discretized by a block of 8 spins in a 5×5 periodic unit cell (i.e., the rows containing 2-4-2 white spins in Fig. 7), the D[II] and D[III] spin configurations result from an increase in the resolution or discretization of this diamond pattern in 7×7 (18 spins: 2-4-6-4-2) and 10×10 (24 spins: 4-4-8-8-4-4) periodic unit cells, respectively. Each of these diamond wallpaper spin configurations were determined to be class I solutions (i.e., unique ground states) and serve to illustrate that the solution class corresponding to a given spin configuration seems to be invariant to a change in the resolution (i.e., an increase or decrease in the discretization or pixelation) of a spin pattern.

As a model for complex pattern recognition, we also considered a simple discretization of an asymmetric facial pattern (see Fig. 8). Unlike the striped-phase, block checkerboard,

and diamond wallpaper spin configurations, this facial pattern has no global symmetry (i.e., no translations, rotations, or reflections leave this spin configuration invariant) and it was found that this spin configuration is an example of a class III solution. Although we have amassed some evidence (*via* the consideration of the facial pattern spin configuration as well as several others) that there seems to be a prevalence of class III solutions among spin configurations with a lack of global symmetry and long-range order, the intrinsic symmetry (or lack thereof) of a spin configuration alone is not enough to make an *a priori* prediction of the solution class corresponding to a given target spin configuration. As an example, Fig. 9 depicts the simplest and lowest-symmetry spin configuration (within a fundamental 2×2 periodic cell) that yields a class III solution.

IV. MAPPING SPIN CONFIGURATIONAL SPACE ONTO THE S_2 CORRELATION FUNCTION

A. Simple spin-spin interaction potentials: Nearest neighbors

When the spin-spin interaction potential is limited to nearest neighbors ($R_{ij} = 1$) only, as in the simplest Ising model [cf. Eq. (1)], there are two possible *unique* ground-state spin
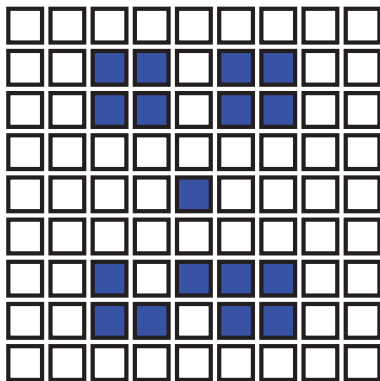

FIG. 8. (Color online) Graphical depiction of a discretized asymmetric facial spin pattern considered in this work. With no global symmetry or long-range order, this spin configuration is an example of a class III solution.
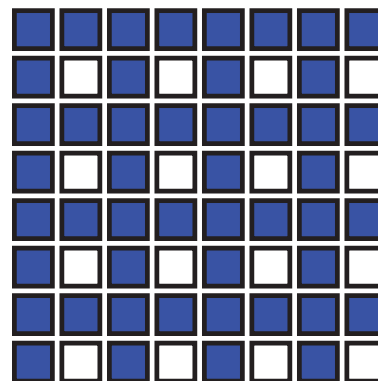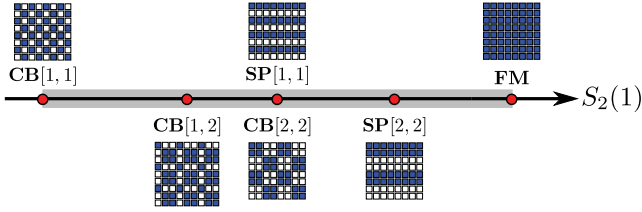

FIG. 9. (Color online) Graphical depiction of the simplest and lowest-symmetry spin configuration (within a fundamental 2×2 periodic cell) that yields a class III solution.

FIG. 10. (Color online) Nearest-neighbor $\mathbf{S}_2$ values for a select subset of spin configurations. From left to right, the corresponding $[S_2(1)]$ values are as follows: CB[1,1], (-2); CB[1,2], $(-2/3)$; SP[1,1] and CB[2,2], (0); SP[2,2], (1); and FM, (2). Between the extremal values of ± 2, the light gray shading represents the nearest-neighbor S_2 values for the *entire spectrum* of possible spin configurations discretized on a periodic square lattice.

configurations (class I solutions): the classic antiferromagnetic (CB[1,1]) and ferromagnetic (FM) spin configurations, which correspond, respectively, to the left and right end points of the line depicting the *entire spectrum* of spin configurations (discretized on a periodic square lattice) existing on the $S_2(1)$ axis in Fig. 10.

With each spin antialigned with respect to its nearest neighbors, the antiferromagnetic CB[1,1], or simple checkerboard, spin configuration has $\mathbf{S}_2 = (-2)$ and is the unique ground state corresponding to an optimized spin-spin interaction potential of $\mathbf{J} = (-1)$. The ferromagnetic FM spin configuration, on the other hand, is comprised of a system of fully aligned spins (i.e., either $\sigma_i = +1$ or $\sigma_i = -1 \; \forall \; i$) with $\mathbf{S}_2 = (+2)$ and is the unique ground state corresponding to an optimized spin-spin interaction potential of $\mathbf{J} = (+1)$. In both of these cases, the magnitude of the observed $\mathbf{S}_2 = (\mp 2)$ values is actually the maximum (absolute value) for the $S_2(1)$ component, a reflection of the nearest-neighbor coordination degeneracy on the square lattice [cf. Eqs. (4) and (8)]. Since the $J(R)$ are bounded within the interval $[-1,+1]$, each of these spin configurations can therefore attain the lowest allowed energetic value when the corresponding nearest-neighbor interaction potential is also extremal at $\mathbf{J} = (\mp 1)$, respectively [cf. Eq. (5)]. From the competitor-based optimization point of view, these nearest-neighbor interaction potentials maximize the energetic gap $\Delta \epsilon^k$ between the corresponding target spin configurations and all possible competitors, and hence the objective function in Eq. (7).

The optimized nearest-neighbor interaction potentials for the CB[1,1] and FM spin configurations can also be analyzed by considering a given nearest-neighbor interaction potential as the projection of the vector $\mathbf{J}$ along the $S_2(1)$ axis in Fig. 10. In this case, finding the unique ground-state spin configuration (class I solution) corresponding to a given interaction potential is accomplished by locating the spin configuration with the $\mathbf{S}_2$ that minimizes the energy per spin expression $\epsilon = -\mathbf{J} \cdot \mathbf{S}_2 = -J(1)S_2(1)$ given in Eq. (5). For the antiferromagnetic $\mathbf{J} = (-1)$ nearest-neighbor interaction potential, which points to the left on the $S_2(1)$ axis, one can clearly see from Fig. 10 that the CB[1,1] spin configuration with $\mathbf{S}_2 = (-2)$ represents the extremal point along the negative $S_2(1)$ axis; hence, the CB[1,1] spin configuration minimizes the energy expression for the antiferromagnetic nearest-neighbor interaction potential, and is therefore the unique ground-state spin

configuration corresponding to this interaction potential. In the same vein, the FM spin configuration is the unique ground-state spin configuration corresponding to the ferromagnetic $\mathbf{J} = (+1)$ nearest-neighbor interaction potential, as this spin configuration is located at the extremum of the positive $S_2(1)$ axis with $\mathbf{S}_2 = (+2)$.

However, the existence of only two possible unique ground-state spin configurations (class I solutions) at the level of nearest-neighbor interactions is not contingent upon the interaction potential assuming the extremal values of $\mathbf{J} = (\pm 1)$. For instance, the infinite number of nearest-neighbor interaction potentials given by $\mathbf{J} \in [-1,0)$ and $\mathbf{J} \in (0, +1]$, which point to the left and right along the $S_2(1)$ axis in Fig. 10 accordingly, will also yield the CB[1,1] and FM spin configurations as unique ground states, respectively. Since these spin configurations represent the extremal values on the $S_2(1)$ axis, only these spin configurations can attain the minimum allowed energy values for the aforementioned interaction potentials. The only exception in this case occurs for the null nearest-neighbor interaction potential [i.e., $\mathbf{J} = (0)$], in which *all* spin configurations are degenerate with $E = 0$, i.e., such an interaction potential is unable to favor any one spin configuration and therefore can not energetically discriminate amongst them (class III solution).

B. Simple spin-spin interaction potentials: Nearest and next-nearest neighbors

When the spin-spin interaction potential is extended to include next-nearest neighbors as well, an additional unique ground state (class I solution) emerges: the simple striped-phase (SP[1,1]) spin configuration, the lower vertex of the triangle depicting the *entire spectrum* of spin configurations (discretized on a periodic square lattice) existing on the $S_2(1)$-$S_2(\sqrt{2})$ plane in Fig. 11. The SP[1,1] striped-phase spin configuration has $\mathbf{S}_2 = (0, -2)$ [i.e., $S_2(1) = 0$ and $S_2(\sqrt{2}) = -2$] since each spin has two aligned and two antialigned spins for its nearest neighbors while its next-nearest neighbors are always antialigned. As such, the SP[1,1] spin configuration, with an extremal value of $S_2(R)$ for the next-nearest-neighbor interspin separation of $R = \sqrt{2}$, was found to be the unique ground-state spin configuration corresponding to an optimized interaction potential of $\mathbf{J} = (0, -1)$.

In order for the SP[1,1] spin configuration to exist as a unique ground state (class I solution) at the level of nearest- and next-nearest-neighbor interactions, the corresponding interaction potential must *simultaneously* energetically favor the SP[1,1] target spin configuration while energetically disfavoring all other spin configurations, in particular the strongly competitive CB[1,1] and FM spin configurations, which now correspond to the upper left and right vertices of the triangle depicted in Fig. 11, respectively.

At the level of nearest-neighbor interactions, the CB[1,1] and FM spin configurations have $S_2(1) = -2$ and $S_2(1) = +2$, respectively, which are in stark contrast to the null value of $S_2(1) = 0$ found for the SP[1,1] spin configuration. As such, there is no nearest-neighbor component of the interaction potential that can favor the SP[1,1] spin configuration over the CB[1,1] and FM spin configurations. Hence, the optimized interaction potential corresponding to the SP[1,1] spin
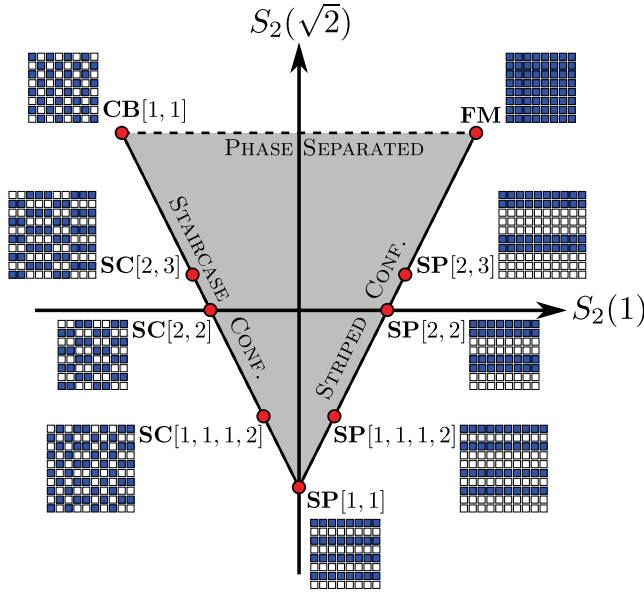
FIG. 11. (Color online) Graphical depiction of the nearest- and next-nearest neighbor S_2 values for a select subset of spin configurations. Clockwise from the upper left-hand vertex, the corresponding $[S_2(1), S_2(\sqrt{2})]$ values are as follows: CB[1,1], $(-2,2)$; FM, $(2,2)$; SP[2,3], $(6/5,2/5)$; SP[2,2], $(1,0)$; SP[1,1,1,2], $(2/5,-6/5)$; SP[1,1], $(0,-2)$; SC[1,1,1,2] (Ref. 46), $(-2/5,-6/5)$; SC[2,2], $(-1,0)$; SC[2,3], $(-6/5,2/5)$. Within the triangle delineated by vertices at $(-2,2)$, $(2,2)$, and $(-1,0)$, the light gray shading represents the nearest- and next-nearest-neighbor S_2 values for the *entire spectrum* of possible spin configurations discretized on a periodic square lattice.

configuration must first minimize the latent energetic stabilization that can be accessed by nearest-neighbor interactions in both the CB[1,1] and FM spin configurations; in this case, this is most easily accomplished by nullifying all nearest-neighbor interactions so that $J(1) = 0$.

At the level of next-nearest-neighbor interactions, the CB[1,1] and FM spin configurations both have $S_2(\sqrt{2}) = +2$, again extremal for this interspin separation, but opposite in sign to the $S_2(\sqrt{2}) = -2$ value found for the SP[1,1] spin configuration. Given these values of $S_2(\sqrt{2})$, the optimized interaction potential corresponding to the SP[1,1] spin configuration admits antiferromagnetic next-nearest-neighbor interactions at full interaction strength, i.e., with $J(\sqrt{2}) = -1$, since this simultaneously maximizes the energetic stabilization provided by next-nearest-neighbor interactions in the SP[1,1] spin configuration while minimizing the energetic stabilization provided by next-nearest-neighbor interactions in both the CB[1,1] and FM spin configurations. From Eq. (5), it is clear that the $\mathbf{J} = (0, -1)$ interaction potential will energetically favor the SP[1,1] spin configuration and maximize the energetic gap between the simple striped-phase spin configuration and the competing ferromagnetic and antiferromagnetic Ising spin magnets [cf. Eq. (7)].

At the level of nearest- and next-nearest-neighbor interactions, the optimized interaction potential for the SP[1,1] spin configuration can also be explained by considering this interaction potential as the projection of the vector $\mathbf{J}$ onto the $S_2(1)$-$S_2(\sqrt{2})$ plane [i.e., $\mathbf{J} = (0, -1)$] as depicted in Fig. 11.

Since the projection of this vector is collinear with the $S_2(\sqrt{2})$ axis, it is clear that the SP[1,1] spin configuration, with $S_2(\sqrt{2}) = -2$, will minimize the energy expression in Eq. (5) given $\mathbf{J} = (0, -1)$, yielding the SP[1,1] spin configuration as the corresponding unique ground state of this interaction potential.

As discussed above for the simple nearest-neighbor interaction potential, there exists some leeway in the interaction potential vectors that will yield the SP[1,1] spin configuration as a corresponding unique ground state (class I solution). In this case, the interaction potential must balance (i) the energetic stabilization that can be afforded to all other spin configurations at the level of nearest-neighbor interactions, i.e., when the projection of the interaction potential vector onto the $S_2(1)$ axis is nonzero, and (ii) the energetic destabilization of the SP[1,1] spin configuration resulting from an antiferromagnetic next-nearest-neighbor interaction that is not extremal, i.e., for $J(\sqrt{2}) \in (0, -1)$. The infinite set of interaction potential vectors that are able to successfully balance these energetic contributions are located *within* the arc (with a central angle of $\theta = \cos^{-1} -3/5 = 126.9°$) formed by the vectors normal to the left edge (connecting SP[1,1] and CB[1,1]) and right edge (connecting SP[1,1] and FM) in Fig. 11.

An important point to note here is that interaction potentials that are equivalent to the vectors normal to the left $[\mathbf{J} = (-1, -1/2)]$ and right $[\mathbf{J} = (1, -1/2)]$ edges will not correspond to a unique ground-state spin configuration (class I solution). For these specific interaction potentials, *all* of the spin configurations located on the respective edge, i.e., the staircase[46] (SC) and striped-phase (SP) spin configurations, respectively, will be energetically degenerate, therefore leading to a class III solution. Furthermore, the spin configurations located within the shaded interior of the triangle in Fig. 11, which includes all other possible spin configurations that can be discretized on a periodic square lattice, can never be ground states (either unique or nonunique) for radial spin-spin interaction potentials that are only nonzero at the level of nearest and next-nearest neighbors.

V. CONCLUSIONS AND FUTURE OUTLOOK

The primary motivation behind the research reported herein was to determine the capacity of the statistical-mechanical "inverse method" to produce preselected, or target, spin configurations (patterns) as classical ground-state structures, using only radial (isotropic) pairwise spin-spin interaction potentials with a minimum finite range. For practical purposes, this initial foray into the inverse Ising spin problem has been limited to the 2D square lattice subject to periodic boundary conditions. Detailed analysis of the results has established that the striped-phase (SP) and diamond (D) families of spin configurations provide examples of achievable nondegenerate (unique) ground states (i.e., class I solutions). However, analogous detailed study has revealed that the block checkerboard (CB) family of spin configurations (with the exception of the simplest version, the classic antiferromagnetic Ising model) inevitably leads to finite-order degenerate ground states (i.e., class II solutions). This work has also uncovered

cases of spin configurations that can not serve as classical ground states for finite-range isotropic pairwise interaction potentials, without having non-S_2-type degeneracies. This set of results demonstrates that such interactions have an important but limited capacity to solve "inverse method" problems in classical statistical mechanics. In addition, one of the most notable insights has been that the type and extent of symmetries exhibited by a target spin configuration are not usefully correlated with the ability to make it the nondegenerate classical ground state of a radial pairwise interaction potential.

The entire collection of inverse problems presented by many-spin systems arranged on an underlying periodic array is enormous. This class of problems includes many directions for extending the analysis developed in this paper, and can legitimately serve as subjects for future investigation. However, in the interests of clarity and relative simplicity, the following remarks will be confined to the family of 2D square lattice systems examined above, with interaction potentials described by Eqs. (3)–(5). Nevertheless, even with these restrictions, a considerable collection of basic problems still remains to be addressed by future research.

For one, spin pattern enumeration presents a significant and prominent challenge. One elementary question to ask is how many distinct "primary patterns" of Ising spins can actually exist on an $a \times a$ square lattice comprised of N spins, subject as usual to standard periodic boundary conditions. In this case, a "primary pattern" includes the set of spin configurations that are equivalent up to translations, rotations, reflections, and spin inversion operations. In addition, a primary pattern is also defined so as to exclude it from being formed by periodic replication of a smaller primary pattern that resides on a $b \times b$ lattice, where b is a divisor of a. Note, however, that this requirement does not exclude reduction of a given primary pattern to smaller periodic unit cells of size $b \times c$ where $b \neq c$. It should also be remarked in passing that increasing the lattice resolution of a given primary pattern (e.g., replacing each original lattice site and spin by a 2×2 array of four sites and four Ising spins of the same spin polarization) converts that initial primary pattern to another primary pattern of the correspondingly expanded size.

The basic enumeration questions that follow are how many distinct primary patterns $P(N = a^2)$ exist for a given system size N, and how does that number behave asymptotically in the large system limit? Straightforward counting for small N reveals that

$$P(1) = 1, \quad P(4) = 3, \quad P(9) = 13,$$
$$P(16) = 428, \quad P(25) = 86\,055, \quad \ldots$$

apparently indicating the beginning of a monotonically increasing function of N. It would be useful just to establish qualitatively whether or not the large-N behavior of $P(N)$ involves an exponential increase.

The target spin configurations that were considered throughout this work and separated into class I, II, and III solutions were not necessarily restricted to primary patterns. However, the SP[m,n] striped-phase and the CB[m,n] block checkerboard spin configurations (Figs. 1 and 2), as well as the corresponding CB degenerate structures (contained for

example within the periodically extended structures of Figs. 3 and 4), are indeed formed from primary patterns. The same is true of the basic repeat units for the diamond wallpaper spin configurations (Fig. 7).

This overall primary pattern enumeration naturally resolves into components for each solution class (i.e., classes I, II, and III) as

$$P(N) = P_{\mathrm{I}}(N) + P_{\mathrm{II}}(N) + P_{\mathrm{III}}(N). \quad (10)$$

If indeed this total number rises exponentially with increasing N, then it seems reasonable to speculate that the ratio $P_{\mathrm{I}}(N)/P(N)$ approaches zero as $N \to \infty$ because the number of adjustable radial pairwise spin-spin interactions within the range available for the inverse process of interest only rises algebraically with increasing N. Our research to date indicates that the SP[n,n] striped-phase spin configurations (and certain SP[m,n] spin configurations as explained in Sec. III C) supply class I primary pattern solutions of arbitrarily large size, but the question remains unanswered as to whether or not these are the only contributors to $P_{\mathrm{I}}(N)$ in the large-N asymptotic regime. Furthermore, based on our current findings and previous results on the structural degeneracies of disordered binary two-phase media[47] (which can be mapped to two-state spin systems), it also seems reasonable to conjecture that the number of target spin configurations contained in $P_{\mathrm{I}}(N)$ that lack any global symmetries and long-range order would also asymptotically go to zero in the large system size limit.

With respect to the class II solutions, it also remains to be determined how the ratio $P_{\mathrm{II}}(N)/P(N)$ behaves with increasing N; however, the evidence that is currently available is insufficient to formulate a confident speculation. One possibility is that this ratio remains greater than zero as the system size increases without bound, due to the rapid rise in the number of class II solutions with N, as suggested by the CB[n,n] results reported above in Sec. III B. A more "conservative" possibility is that this ratio converges to zero, but for all N there exists a slowly increasing number of distinct groups of degenerate (class II) primary patterns.

Each of the CB[n,n] structures and their respective S_2-type degeneracies (as illustrated in Figs. 3 and 4 for the simple cases of $n = 2$ and 4) exhibit up and down spins that are equal in number and arranged spatially in equivalent patterns, i.e., structures that have much higher symmetry and order than other well-known disordered degenerate spin configurations.[48–50] Consequently, in any one of these spin configurations the spatial distributions of all orders for just the up spins or just the down spins must be identical. In this regard, the lattice gas interpretation of an Ising spin configuration would formally replace each spin variable σ_i with a site-occupancy variable

$$\xi_i = (\sigma_i + 1)/2. \quad (11)$$

Then, a lattice site i is denoted as occupied by a lattice-gas particle or empty (vacant) if $\xi_i = 1$ or 0, respectively. The identity of $S_2(R)$ for all $g(n)$ degeneracies of the CB[n,n] spin configurations implies that the radial pair distributions for lattice gas molecules, which is straightforwardly obtained from Eqs. (4) and (11), are identical for all of those spin configurations, at least up to the range of the interaction potential (which has been shown in Table II to be n times the lattice spacing).

In other words, within the range of the interaction potential, the distributions of scalar distances between pairs of occupied sites are identical for all CB[n,n] spin configurations and their respective S_2-type degeneracies. With this observation as a stimulus, a numerical study was carried out establishing for spin configurations with $n \leqslant 50$ that the identity of the scalar pair distance distributions between particle-occupied sites in fact extends to the 300th coordination shell; by reasonable extrapolation this may indeed be true for all distances within the infinite periodic structures. It should also not escape notice that such a conclusion about pair-distance degeneracy among distinct periodic patterns on lattices automatically carries over to the study of pair-distance degeneracy in Euclidean spaces.[51]

The focus of the original Ising model with nearest-neighbor interactions was the determination of its thermodynamic properties in the macroscopic regime.[52] The existence of S_2-type degeneracies (i.e., class II solutions) among primary patterns on the square lattice leads to possible generalizations of the relatively simple phase behavior exhibited by the original Ising model with short-range (nearest-neighbor) interactions. In particular, one can periodically replicate each of a set of small class II primary patterns into the macroscopic regime, and then inquire about the thermodynamic and order-parameter behaviors that are produced by the interaction potential involved as the temperature varies. Is there a positive-temperature critical point below which one of the degenerate spin configurations dominates? Alternatively, does the ground-state degeneracy and its resulting structural ambiguity cause critical behavior to be depressed to absolute zero temperature with a nonzero configurational disorder remaining? Such residual disorder (entropy) at absolute zero would be analogous to, but distinct from, that known to occur from frustrated antiferromagnetism on the triangular lattice.[53] The S_2-type degeneracies indicated earlier in Figs. 3 and 4 could therefore serve as starting points for specific analytical and/or numerical examinations of these currently unsettled issues. In particular, it would be quite illuminating to determine the low-lying excited states for each of these degenerate primary patterns, and to see if their presence tends to diminish statistically the geometrical distinctions between those degenerate ground states.

APPENDIX A: CLASS DETERMINATION USING A FINITE SUBSET OF COMPETITORS

In this Appendix, we demonstrate that the solution class corresponding to a given *target* spin configuration $\mathscr{T}$ can be determined by only searching for possible competitor spin configurations that exist on a subset of lattice sizes (as determined by the periodicity of $\mathscr{T}$). To proceed, let us

first assume that $S_2^{\mathscr{T}}(R)$, as defined in Eq. (4), takes on the maximum allowed value at some radial interspin separation $R_{\max}$, i.e., $S_2^{\mathscr{T}}(R_{\max}) = S_2^{\max}(R_{\max})$. In order for $S_2^{\mathscr{T}}(R_{\max})$ to attain this maximum value, all of the spins in $\mathscr{T}$ that are separated by a distance $R_{\max}$ must be aligned. This implies that $\mathscr{T}$ is invariant under translations by any integer vector $\mathbf{R}$ with a length equal to $R_{\max}$. Hence, $\mathscr{T}$ can be represented as a periodic configuration with lattice vectors chosen in $\{\mathbf{R} \in \mathbb{Z}^2 : |\mathbf{R}| = R_{\max}\}$.

Furthermore, let us also suppose that we have identified an interaction potential $\mathbf{J}$ that corresponds to $\mathscr{T}$ having the lowest energy in the subset of all possible spin configurations that also have a maximal value of $S_2(R_{\max})$. This is sufficient evidence that $\mathscr{T}$ is a class I solution (i.e., a unique ground state corresponding to $\mathbf{J}$). This can easily be seen by considering the case where a possible competitor spin configuration C for which $S_2(R_{\max}) < S_2^{\max}(R_{\max})$ has an energy that is lower than (or equal to) the energy of $\mathscr{T}$ using the interaction potential $\mathbf{J}$. In this case, one can simply replace this interaction potential with the following updated potential $J'(R) = J(R) - \eta \delta_{R,R_{\max}}$, in which η is chosen such that C has a higher energy than $\mathscr{T}$. Such a procedure can then be repeated until the interaction potential with $\mathscr{T}$ as the corresponding unique ground state is obtained, i.e., as a class I solution. The same argument also holds for class II solutions since any possible competitor spin configuration with an S_2 that is identical to $\mathscr{T}$ (i.e., an S_2-type degeneracy) will also have a maximal value of $S_2(R_{\max})$ by definition. The determination of the remaining class III solutions, which are those that are not contained in either class I or II, follows by process of elimination.

All of the target spin configurations considered in this work can be represented as periodic configurations on an underlying $a \times a$ square lattice. For the cases in which the only lattice vectors with length $|\mathbf{R}| = a$ are given by $\mathbf{R} = (\pm a, 0)$ and $\mathbf{R} = (0, \pm a)$, these target spin configurations will have a maximal value of $S_2(R_{\max} = a)$. Hence, determination of the solution class corresponding to these target spin configurations only requires a search for possible competitor spin configurations over the subset of $a \times a$ periodic configurations.

The situation is slightly more complicated if the distance a can also be obtained by diagonal vectors (i.e., for a that are hypotenuse numbers). For instance, the radial distance $R = 5$ can occur by any of the following lattice vectors: $\mathbf{R} = (\pm 5, 0)$, $\mathbf{R} = (0, \pm 5)$, $\mathbf{R} = (\pm 4, \pm 3)$, or $\mathbf{R} = (\pm 3, \pm 4)$. This results in a maximum value of $S_2^{\max}(a) = 6$, which is *not* guaranteed for a 5×5 periodic spin configuration, and therefore the previous argument can not be used in such a case. Nevertheless, our numerical experiments strongly indicate that accurate solution class determination only requires consideration of all square periodic unit cells of the same size as the target spin configuration. In the case of the aforementioned 5×5 periodic spin configurations, two such unit cells exist: the first is the standard square lattice that is periodic along $(5,0)$ and $(0,5)$, and the other is the "tilted" square lattice that is periodic along $(4, -3)$ and $(3,4)$. As such, possible competitor spin configurations that exist on *both* of these lattices must be considered when determining the solution class corresponding to a target spin configuration with this type of underlying periodicity.

It should be emphasized again here that the procedure outlined in this Appendix can only be utilized to accurately
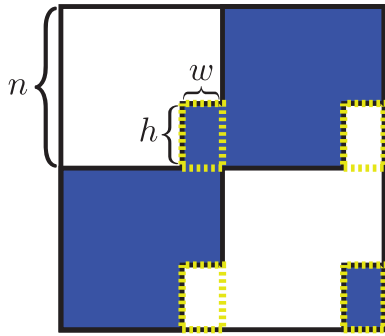
FIG. 12. (Color online) Schematic representation of $CB_{hw}[n,n]$, an S_2-type degeneracy of the $CB[n,n]$ (or $CB_{00}[n,n]$) block checkerboard spin configuration. The spin configuration $CB_{hw}[n,n]$ shares the same $2n \times 2n$ periodicity as the $CB[n,n]$ spin configuration. In addition to n, two parameters are required to identify this S_2-type degeneracy: the height h and the width w of the block of spins that have been flipped in the transformation from $CB[n,n]$ to $CB_{hw}[n,n]$ (highlighted by yellow dashed lines). Note that both h and w are integers between 1 and $n - 1$.

determine the solution class corresponding to a given target spin configuration; any interaction potential obtained in this manner must be verified against *all* possible competitor spin configurations (i.e., spin configurations of different periodicities). Nevertheless, the arguments presented herein indicate that the minimum radial extent of the interaction potential necessary to stabilize a given target spin configuration can not be longer than the distance $R_{\max}$ for which $S_2^{\mathscr{T}}(R_{\max})$ is extremal.

APPENDIX B: ENUMERATION OF THE S_2-TYPE DEGENERACIES OF THE CB[n,n] SPIN CONFIGURATIONS

During the investigation of the sequence of $CB[n,n]$ block checkerboard spin configurations, it was observed that the

S_2-type degeneracies of the $CB[n,n]$ spin configurations (for $n \geqslant 2$) followed a distinct pattern (see Figs. 3 and 4). To construct these S_2-type degeneracies, one starts with the base $CB[n,n]$ block checkerboard spin configuration and identifies all of the corners where four blocks (two blocks of up spins and two blocks of down spins) meet. At each such corner, one then reverses the orientation of the spins in a rectangular region of height h and width w immediately to the top left of the corner. This transformation preserves the overall magnetization of the system since there are an equal number of corners for which the top-left block has either of the two possible spin orientations. In fact, performing the same transformation on any other quadrant would result in an identical spin configuration up to a rotational symmetry operation. Throughout this work, such a spin configuration is denoted as $CB_{hw}[n,n]$, a general example of which is schematically represented in Fig. 12. Using this convention, the $CB[n,n]$ block checkerboard spin configuration can be equivalently denoted as $CB_{00}[n,n]$.

By explicit calculation of $S_2(R)$ (up to the 300th coordination shell), it has been confirmed that all possible $CB_{hw}[n,n]$ spin configurations formed utilizing this prescription are S_2-type degeneracies of their respective $CB_{00}[n,n]$ spin configurations for $2 \leqslant n \leqslant 50$. In addition, we also have strong computational evidence that these are the only S_2-type degeneracies of the $CB_{00}[n,n]$ series, since repeated verification of the optimized interaction potentials through careful simulated annealing has identified these spin configurations.

By determining which values of h and w lead to the same spin configuration, one can enumerate the S_2-type degeneracies of the $CB_{00}[n,n]$ series. As seen in Fig. 12, the exchange of h and w is equivalent to a reflection of the spin configuration about the principal diagonal of the periodic square lattice, which allows us to set $w \leqslant h$ without loss of generality. In addition, one can replace h by $n - h$ and also obtain the same spin configuration. Setting $h \leqslant n/2$ and using both of these conditions, the number of degeneracies $g(n)$ for the $CB[n,n]$ block checkerboard spin configurations leads to Eq. (9) of Sec. III B.

[1] E. Ising, Z. Phys. **31**, 253 (1925).

[2] R. B. Potts, Proc. Cambridge Philos. Soc. **48**, 106 (1952).

[3] C. Domb, J. Phys. A: Math. Nucl. Gen. **7**, 1335 (1974).

[4] J. Ashkin and E. Teller, Phys. Rev. **64**, 178 (1943).

[5] T. Kihara, Y. Midzuno, and J. Shizume, J. Phys. Soc. Jpn. **9**, 681 (1954).

[6] F. Y. Wu, Rev. Mod. Phys. **54**, 235 (1982).

[7] R. J. Elliott, Phys. Rev. **124**, 346 (1961).

[8] M. E. Fisher and W. Selke, Phys. Rev. Lett. **44**, 1502 (1980).

[9] L. Onsager, Phys. Rev. **65**, 117 (1944).

[10] C. N. Yang, Phys. Rev. **85**, 808 (1952).

[11] B. M. McCoy and T. T. Wu, *The Two-Dimensional Ising Model* (Harvard University Press, Cambridge, MA, 1973).

[12] R. J. Baxter, *Exactly Solved Models in Statistical Mechanics* (Academic, London, 1982).

[13] K. Barros, P. L. Krapivsky, and S. Redner, Phys. Rev. E **80**, 040101 (2009).

[14] H. Cohn and Y. Zhao, arXiv:1212.1913.

[15] M. C. Rechtsman, F. H. Stillinger, and S. Torquato, Phys. Rev. E **73**, 011406 (2006).

[16] S. Torquato, Soft Matter **5**, 1157 (2009).

[17] É. Marcotte, F. H. Stillinger, and S. Torquato, J. Chem. Phys. **134**, 164105 (2011).

[18] É. Marcotte, F. H. Stillinger, and S. Torquato, J. Chem. Phys. **138**, 061101 (2013).

[19] M. C. Rechtsman, F. H. Stillinger, and S. Torquato, J. Phys. Chem. A **111**, 12816 (2007).

[20] M. C. Rechtsman, F. H. Stillinger, and S. Torquato, Phys. Rev. Lett. **101**, 085501 (2008).

[21] In the summation in Eq. (3), the index i runs over spins contained in the periodic unit cell while the index j runs over spins contained in both the periodic unit cell and its images.

[22] For a given periodic system with a unit cell containing N spins, $S_2(R)$ and the spin-spin correlation function $s(R)$ are related via $s(R) = \frac{1}{N \times N_R} \sum_{i<j} \sigma_i \sigma_j \delta_{R,R_{ij}} = \frac{1}{N_R} S_2(R)$, where N_R is the number of unique pairs of spins separated by the distance R.

[23] As such, Class III solutions include the trivial case of $J(R) = 0 \forall R$, with an $E = 0$ degeneracy for *any* spin configuration.

[24] M. Seul and R. Wolfe, Phys. Rev. A **46**, 7519 (1992).

[25] F. Ancilotto and A. Selloni, Phys. Rev. Lett. **68**, 2640 (1992).

[26] R. Allenspach, M. Stampanoni, and A. Bischof, Phys. Rev. Lett. **65**, 3344 (1990).

[27] R. Allenspach and A. Bischof, Phys. Rev. Lett. **69**, 3385 (1992).

[28] K. Kern, H. Niehus, A. Schatz, P. Zeppenfeld, J. Goerge, and G. Comsa, Phys. Rev. Lett. **67**, 855 (1991).

[29] H. Mohwald, Thin Solid Films **159**, 1 (1988).

[30] S. L. Keller and H. M. McConnell, Phys. Rev. Lett. **82**, 1602 (1999).

[31] J. Maclennan and M. Seul, Phys. Rev. Lett. **69**, 2082 (1992).

[32] C. Harrison, D. H. Adamson, Z. Cheng, J. M. Sebastian, S. Sethuraman, D. A. Huse, R. A. Register, and P. M. Chaikin, Science **290**, 1558 (2000).

[33] J. M. Tranquada, D. J. Buttrey, V. Sachan, and J. E. Lorenzo, Phys. Rev. Lett. **73**, 1003 (1994).

[34] J. M. Tranquada, B. J. Sternlieb, J. D. Axe, Y. Nakamura, and S. Uchida, Nature (London) **375**, 561 (1995).

[35] V. J. Emery, S. A. Kivelson, and J. M. Tranquada, Proc. Natl. Acad. Sci. USA **96**, 8814 (1999).

[36] W. S. Choi, J.-H. Kwon, H. Jeen, J. E. Hamann-Borrero, A. Radi, S. Macke, R. Sutarto, F. He, G. A. Sawatzky, V. Hinkov, M. Kim, and H. N. Lee, Nano Lett. **12**, 4966 (2012).

[37] A. Giuliani, J. L. Lebowitz, and E. H. Lieb, Phys. Rev. B **74**, 064420 (2006).

[38] A. Giuliani, J. L. Lebowitz, and E. H. Lieb, Phys. Rev. B **76**, 184426 (2007).

[39] A. Giuliani, J. L. Lebowitz, and E. H. Lieb, Phys. Rev. B **84**, 064205 (2011); Commun. Math. Phys. **286**, 163 (2009).

[40] A. Giuliani, E. H. Lieb, and R. Seiringer, Phys. Rev. B **88**, 064401 (2013).

[41] R. B. Batten, D. A. Huse, F. H. Stillinger, and S. Torquato, Soft Matter **7**, 6194 (2011).

[42] H. Cohn and A. Kumar, Proc. Natl. Acad. Sci. USA **106**, 9570 (2009).

[43] J. H. Conway and N. J. A. Sloane, *Sphere Packings, Lattices, and Groups* (Springer, New York, 1993).

[44] R. J. Vanderbei, *Linear Programming: Foundations and Extensions* (Springer, New York, 2008).

[45] S. Kirkpatrick, C. D. Gelatt, and M. P. Vecchi, Science **220**, 671 (1983).

[46] The staircase (SC) spin configurations can be generated from the striped-phase (SP) spin configurations utilizing the following "gauge" transformation $\sigma_{x,y}^{SC} = (-1)^{x+y} \sigma_{x,y}^{SP}$, a consequence of which is the fact that $S_2^{SC}(R) = (-1)^{R^2} S_2^{SP}(R)$. Hence, all of the conclusions reached throughout this work regarding the striped-phase spin configurations can be straightforwardly applied to the corresponding staircase spin configurations.

[47] C. J. Gommes, Y. Jiao, and S. Torquato, Phys. Rev. Lett. **108**, 080601 (2012).

[48] J. Snyder, J. S. Slusky, R. J. Cava, and P. Schiffer, Nature (London) **413**, 48 (2001).

[49] S. V. Isakov, R. Moessner, and S. L. Sondhi, Phys. Rev. Lett. **95**, 217201 (2005).

[50] C. L. Henley, Annu. Rev. Condens. Matter Phys. **1**, 179 (2010).

[51] Y. Jiao, F. H. Stillinger, and S. Torquato, Phys. Rev. E **81**, 011105 (2010).

[52] K. Huang, *Statistical Mechanics* (Wiley, New York, 1963).

[53] G. H. Wannier, Phys. Rev. **79**, 357 (1950).